Journal of Magnetism and Magnetic Materials 477 (2019) 198–202

Contents lists available at ScienceDirect

Journal of Magnetism and Magnetic Materials

journal homepage: www.elsevier.com/locate/jmmm

Research articles

Modelling the effect of different core sizes and magnetic interactions inside magnetic nanoparticles on hyperthermia performance

Christian Jonasson[a,*], Vincent Schaller[a], Lunjie Zeng[b], Eva Olsson[b], Cathrine Frandsen[c], Alejandra Castro[d], Lars Nilsson[d], Lara K. Bogart[e], Paul Southern[e], Quentin A. Pankhurst[e], M. Puerto Morales[f], Christer Johansson[a]

[a] RISE Acreo, Göteborg, Sweden
[b] Department of Physics, Chalmers University of Technology, Göteborg, Sweden
[c] Department of Physics, Technical University of Denmark, Kgs. Lyngby, Denmark
[d] Solve AB, Lund, Sweden
[e] UCL Healthcare Biomagnetics Laboratory, University College London, UK
[f] Institute of Material Science of Madrid (ICMM-CSIC), Madrid, Spain

ARTICLE INFO

Keywords:
Magnetic nanoparticles
Magnetic interactions
Magnetic relaxation
Monte-Carlo simulations
Multi-core particles
Single-core particles

ABSTRACT

We present experimental intrinsic loss power (ILP) values, measured at an excitation frequency of 1 MHz and at relatively low field amplitudes of 3.4–9.9 kA/m, as a function of the mean core diameter, for selected magnetic nanoparticles (MNPs). The mean core sizes ranged from ca. 8 nm to 31 nm. Transmission electron microscopy indicated that those with smaller core sizes (less than ca. 22 nm) were single-core MNPs, while those with larger core sizes (ca. 29 nm to 31 nm) were multi-core MNPs. The ILP data showed a peak at core sizes of ca. 20 nm. We show here that this behaviour correlates well with the predicted ILP values obtained using either a non-interacting Debye model, or via dynamic Monte-Carlo simulations, the latter including core-core magnetic interactions for the multi-core particles. This alignment of the models is a consequence of the low field amplitudes used. We also present interesting results showing that the core-core interactions affect the ILP value differently depending on the mean core size.

1. Introduction

Iron oxide based magnetic nanoparticles (MNPs) are already being used in several biomedical applications such as diagnosis, actuation, imaging and therapy [1,2]. One interesting and promising *in-vivo* MNP application is magnetic hyperthermia for cancer therapy [3], for which the figures of merit are the specific loss power (SLP) or intrinsic loss power (ILP) parameters, both of which characterise the heating performance of a given MNP sample.

In a recent EU-funded project (NanoMag), we have studied ca. 50 different iron oxide MNP systems with the goal of improving our metrological understanding of this class of materials. These have been both single-core and multi-core MNP systems, with different core sizes, core packing density and number of cores per core-cluster. For further details on the single-core and multi-core particle structure and terminology see [4].

The data obtained on both single-core and multi-core MNPs is interesting in the context of magnetic hyperthermia, given that it has been reported previously that ILP values may be dependent on the strength of magnetic core-core interactions, with stronger interactions leading to lower ILPs [5]. This implies that the ILP should be lower in multi-core MNPs than in corresponding single-core MNPs, due to the core-core interactions.

In this study we compare the measured ILP values in selected particles with both a non-interacting Debye model and with dynamic Monte-Carlo simulations including, for multi-core particles, core-core magnetic interactions.

We have earlier made substantial static Monte-Carlo simulations where we introduced anisotropy energies and dipolar-dipolar interactions between the cores in multi-core particles and where we also included core size distribution as well as varying the easy-axis distribution [6–8]. In these studies, the energies can be independently introduced in order to study their different contribution to the magnetic response.

In this study we have further developed this static equilibrium simulation to a dynamic Monte-Carlo model by studying the probabilities

* Corresponding author.
E-mail address: christian.jonasson@ri.se (C. Jonasson).

https://doi.org/10.1016/j.jmmm.2018.09.117
Received 24 June 2018; Received in revised form 17 September 2018; Accepted 28 September 2018
Available online 03 October 2018
0304-8853/

Table 1
Structural details of the studied MNP systems.

MNP system	Type	D_m (nm)	σ_D (nm)
CSIC-01	Single-core	11.6	1.2
CSIC-03	Single-core	7.9	1.6
CSIC-11	Single-core	14.6	1.9
CSIC-12	Single-core	21.7	3.8
CSIC-04	Multi-core	28.7	8.7
CSIC-05	Multi-core	30.7	9.2
CSIC-06	Multi-core	28.7	7.9

of core magnetization switching compared to the frequency of an applied AC magnetic field.

Several other studies on dynamic Monte-Carlo simulations on interacting magnetic nanoparticles have been performed [9–12], but in this study we have compared the simulation results with experimental data for an especially large core size range (ca. 8 nm to ca. 31 nm), and we have paid particular attention to the particle type (single-core or multi-core).

2. Material and methods

2.1. Magnetic nanoparticles

Iron oxide based magnetic nanoparticles were synthesized using different methods to obtain single- and multi-core magnetite particles with different core and cluster sizes. For the single-core particles (CSIC-01, CSIC-03, CSIC-11 and CSIC-12), thermal decomposition of iron oleate in organic media was used as the synthesis route, reducing the amount of oleic acid to increase particle size [13]. The CSIC-01 sample was coated with silica (silica layer of about 9 nm). CSIC-03, CSIC-11 and CSIC-12 MNPs were coated with meso-2,3-dimercaptosuccinic acid (DMSA). The multi-core particles CSIC-04, CSIC-05 and CSIC-06 were synthesized using oxidative precipitation including an acid treatment [14]. These particles produced in one batch were coated with dextran under high pressure homogenization (HPH) conditions and subjected to fractionation leading to multicore particles with different number of cores per particle.

The mean core diameter (D_m), log-normal distribution standard deviation (σ_D) given in nm, and type of MNP system, as determined by transmission electron microscopy (TEM), are given in Table 1.

The mean number of cores building up the core-cluster (as defined in [4]) in each multi-core particle was ca. 2.5, 4.6 and 2.1 for CSIC-04, CSIC-05 and CSIC-06 respectively, as determined by TEM. As a consequence of the different number of cores in the core-clusters, the total cluster size will differ regardless the similar core diameter size. Details on the number of cores per core-cluster and how it has been determined will be reported in [15]. Fig. 1 shows TEM images of the CSIC-04 and CSIC-12 particle systems.

2.2. Experimental

ILP values were measured using a Materials Characterisation MACH system (Resonant Circuits Limited, UK) at an excitation frequency of 1 MHz and at field amplitudes ranging from 3.4 to 9.9 kA/m. The temperature change was measured using fluoroptic probes, and the data were analyzed using the 'corrected slope method' for non-adiabatic systems [16].

TEM was performed using a FEI Titan 80–300 equipped with a field emission gun and operating at 80 or 300 kV.

2.3. Theory

A non-interacting ILP model based on the Debye model and inspired by Rosensweig [17] has been developed. The model takes into account the core size distribution, the field dependence of the relaxation time using the field dependent Néel relaxation time [18,19], as well as an approximation of the non-linear field effects in the out-of-phase magnetization using the Langevin function [17,20]. The ILP is given by:

$$ILP = \frac{\pi\mu_0 M_s}{H_0\rho < V_c >} \int V_c L\left(\frac{M_S V_c \mu_0 H_0}{k_B T}\right) \frac{2\pi f\tau_{eff}}{1 + (2\pi f\tau_{eff})^2} f_{LN}(D_c) dD_c \quad (1)$$

where

$$\frac{1}{\tau_{eff}} = \frac{1}{\tau_N} + \frac{1}{\tau_B}$$

$$\tau_N = \tau_0 exp\left(\frac{KV_c}{k_B T}\left(1 - \frac{H_0}{H_a}\right)^2\right)$$

$$\tau_B = \frac{3V_H\eta}{k_B T}$$

and $L(x)$ is the Langevin function, H_a the anisotropy field equal to$2K/\mu_0 M_S$, K the anisotropy constant, H_0 the field amplitude, f the excitation frequency, M_s the saturation magnetization, f_{LN} the core size distribution (log-normal function), ρ the density of the magnetic core, D_c the core diameter, V_c and $< V_c >$ the core volume and the mean core volume respectively, V_H the hydrodynamic volume of the particle, η is the viscosity of the fluid where the MNPs are dispersed, k_B the Boltzmann constant, τ_N the Néel relaxation time, τ_B the Brownian relaxation time, τ_0 the characteristic relaxation time, and T is the temperature.

A dynamic Monte-Carlo model has also been developed to study the

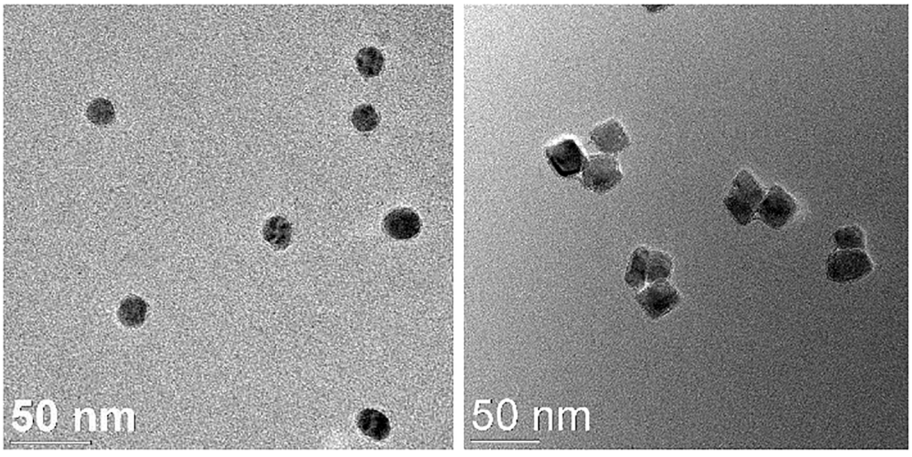

Fig. 1. TEM images showing the single-core particle system CSIC-12 (left) and the multi-core system CSIC-04 (right).

dynamic magnetic response of single- and multi-core particles. We use a two-level approximation of the magnetic energy states inside the cores [10,11]. The unit time of simulation is equal to one Monte-Carlo step (1 mcs) where all cores are updated; 1 mcs corresponds to τ_0 (typically 10^{-9}–10^{-11} s). Multicore particles are built up as core-clusters of N_c spherical cores defined by the number of cores in the cluster, core size distribution, packing density of the cluster, random or aligned easy axis orientation inside each core, and core dead layer thickness [7]. Anisotropy, dipole-dipole, and exchange interactions are all included in the model. The total energy of a spherical core i can be written as:

$$E_i = -KV_i\left(\frac{\boldsymbol{\mu}_i}{|\boldsymbol{\mu}_i|}\cdot\boldsymbol{n}_i\right)^2 - \boldsymbol{\mu}_i\cdot\boldsymbol{B}_i \tag{2}$$

where K is the anisotropy constant, V_i the core volume, $\boldsymbol{\mu}_i$ the magnetic moment of the core with magnitude of $|\boldsymbol{\mu}_i| = M_S V_i$, $\boldsymbol{n}_i$ the unit vector of the easy axis and M_s the saturation magnetization.

The total magnetic field $\boldsymbol{B}_i$ acting on a core i is a sum of the external applied field, the dipolar field from all surrounding cores and the exchange interaction field from the very close neighbours. The total field H_i is given by:

$$\boldsymbol{H}_i = \boldsymbol{H}_{ext} + \sum_j J_{ij}\boldsymbol{\mu}_j - \frac{1}{4\pi}\sum_j\left(\frac{\boldsymbol{\mu}_j}{|\boldsymbol{r}_{ij}|^3} - \frac{3(\boldsymbol{\mu}_j\cdot\boldsymbol{r}_{ij})\boldsymbol{r}_{ij}}{|\boldsymbol{r}_{ij}|^5}\right) \tag{3}$$

where $\boldsymbol{H}_{ext}$ is the applied external field, $\boldsymbol{\mu}_j$ the magnetic moment, $\boldsymbol{r}_{ij}$ the vector between core i and j and J_{ij} is the nearest-neighbor exchange coupling constant between core i and j, defined as $J_{ij} = H_a/VM_s$ (for $D_c = 10$ nm, $J_{ij} = 2.4{\cdot}10^{23}$) [10].

It has been shown that the minimum energy is found when all three vectors, $\boldsymbol{\mu}_i$, $\boldsymbol{n}_i$, and $\boldsymbol{B}_i$ are in the same plane and hence the energy function can be written as:

$$E_i = -KV_i[\cos^2(\alpha_i) + (M_s/K)|\boldsymbol{B}_i|\cos(\varphi_i - \alpha_i)] \tag{4}$$

where α_i is the angle between $\boldsymbol{n}_i$ and $\boldsymbol{\mu}_i$, and φ_i the angle between $\boldsymbol{B}_i$ and $\boldsymbol{n}_i$.

For a given applied field we calculate the energy minima and the saddle point for each core i in the cluster. We assume that the magnetic moment must be aligned with one of the minima and the probability for the moment to flip between the two extreme points is given by the energy barrier related to the thermal energy, according to:

$$p_i = e^{-(E_i^{sad} - E_i^{min})/k_B T}$$

where E_i^{min} is the minimum energy where the moment is located, E_i^{sad} is the saddle point energy, k_B the Boltzmann constant and T is the temperature. The magnetic moment flips if the probability p_i is greater than a drawn random number between 0 and 1.

To simulate the dynamic response from a core-cluster we apply an AC magnetic field, $H_0\sin(\omega t)$. One period of the signal is divided into n discrete points and the total magnetic moment of the cluster is calculated for each field step. The number of Monte-Carlo steps m for each field point is given by the frequency of the applied field f, τ_0 and n. The total magnetic moment for each core-cluster is then averaged over a large number of clusters (typ. order of 1000) and a number of periods (typ. 10 periods) to determine a mean value of the total magnetic moment for the particle system. The results are typically presented as hysteresis loops and the loop area is used to calculate the ILP value.

3. Results and discussion

Using the non-interacting model and $K = 10$ kJ/m^3 [21], $T = 300$ K and a log-normal size distribution width (i.e. standard deviation) of $\sigma = 0.2$ the ILP are calculated and plotted versus the field amplitude and the median core diameter, as visualized in the 3D plot in Fig. 2.

As can be seen from Fig. 2 there is maximum in ILP at a specific core diameter when varying the core size. At this specific core diameter, the mean core relaxation rate is in the same range as the excitation frequency. In the non-interacting model, we assume that the non-linear field behavior of the out-of-phase magnetization can be approximated by the Langevin function and we approximate the field dependence of the Néel relaxation by Eq. (1).

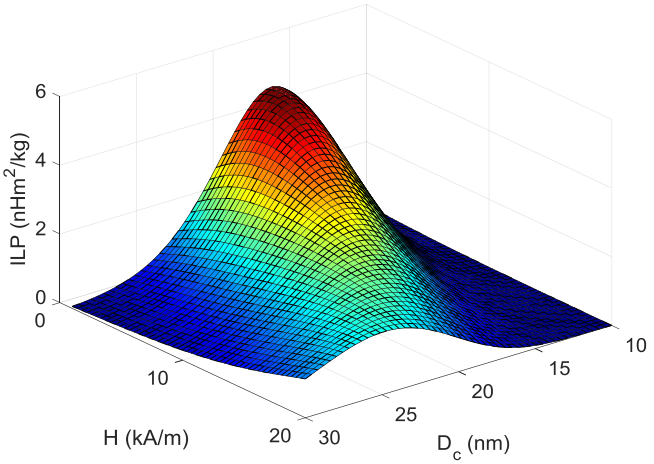

Fig. 2. ILP versus field amplitude and mean core diameter for the following parameters $K = 10$ kJ/m^3, $T = 300$ K, size distribution width $\sigma = 0.2$ (standard deviation) and $\tau_0 = 10^{-10}$ s, only taking the Néel contribution into account. The ILP values are colour coded from blue (low ILP) to red (high ILP). (For interpretation of the references to colour in this figure legend, the reader is referred to the web version of this article.)

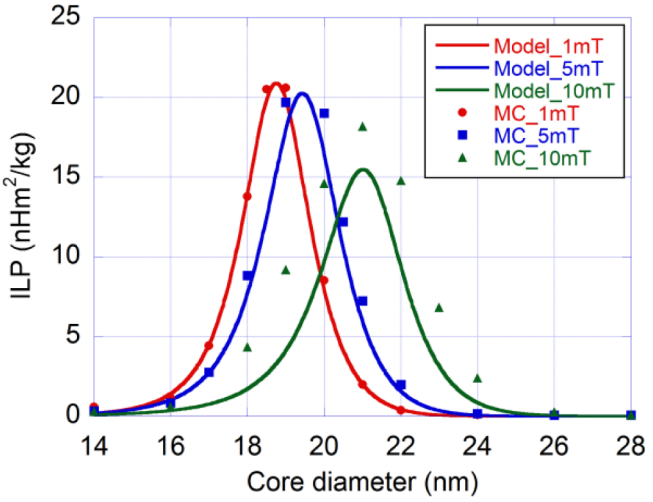

Fig. 3. ILP versus core diameter using the non-interacting model together with the results from the dynamic MC-simulations, for mono-dispersed cores at different field amplitudes (only taking the Néel contribution into account), red: $B_0 = 1$ mT, blue: $B_0 = 5$ mT and green: $B_0 = 10$ mT. $f = 1$ MHz, $K = 10$ kJ/m^3 and $T = 300$ K. "Model" in the legend indicates the result from the non-interaction model and "MC" the result from the dynamic Monte-Carlo simulations. (For interpretation of the references to colour in this figure legend, the reader is referred to the web version of this article.)

To test these assumptions, we used the same parameters in the non-interacting model and in the Monte-Carlo simulations for a mono-dispersed non-interacting MNP case[‡]. The result is plotted in Fig. 3.

As can be seen in Fig. 3 there is good resemblance between the non-interacting model (Eq. (1)) and the dynamic Monte-Carlo simulations. At higher field amplitudes we have some deviations, probably due to

[‡] Note that using the ILP parameter to describe magnetic heating in a monodisperse MNP system is rather an oxymoron, as the ILP is strictly only valid in polydisperse ($\sigma > 0.1$) systems [22]. It is used here for illustration only.

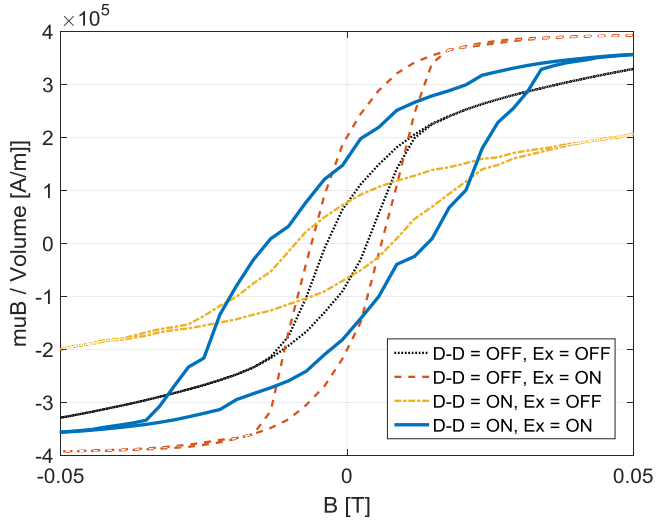

Fig. 4. Simulated hysteresis loops (magnetization vs field) at different interactions by switching ON and OFF dipole-dipole and exchange contributions; Number of cores $N_c = 20$, random closed packed (RCP), $K = 10\,\mathrm{kJ/m^3}$, $M_S = 400\,\mathrm{kA/m}$, $T = 300\,\mathrm{K}$, $D_c = 15\,\mathrm{nm}$. Applied field amplitude and frequency is $B_0 = 50\,\mathrm{mT}$ and $f = 1\,\mathrm{MHz}$. Jumps in the blue curve is due to a limited number of core-clusters used in simulation. This effect is most significant when both types of interactions are included. (For interpretation of the references to colour in this figure legend, the reader is referred to the web version of this article.)

the assumption of using the Langevin function that describes the non-linear field effects for this dynamic magnetic case.

Fig. 4 shows that the different types of interactions give a different behaviour in the hysteresis loop. Dipole-dipole interactions stretch out the hysteresis in field and the exchange interactions stretch out the hysteresis loop in magnetization (for instance increase of the remanence).

From the result showing in Fig. 5 the enclosed area (absorbed energy) increase with field amplitude, as expected.

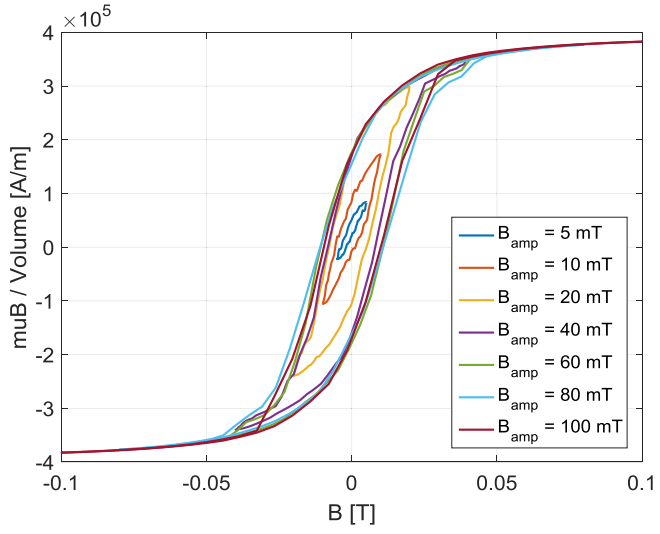

Fig. 5. Simulated hysteresis loops (magnetization vs field) at different field amplitudes as indicated in the figure; using $N_c = 20$ (RCP), $K = 10\,\mathrm{kJ/m^3}$, $M_S = 400\,\mathrm{kA/m}$, $T = 300\,\mathrm{K}$, $D_c = 15\,\mathrm{nm}$. Applied frequency is $f = 1\,\mathrm{MHz}$. Both dipole-dipole interactions and exchange interactions are included. (For interpretation of the references to colour in this figure legend, the reader is referred to the web version of this article.)

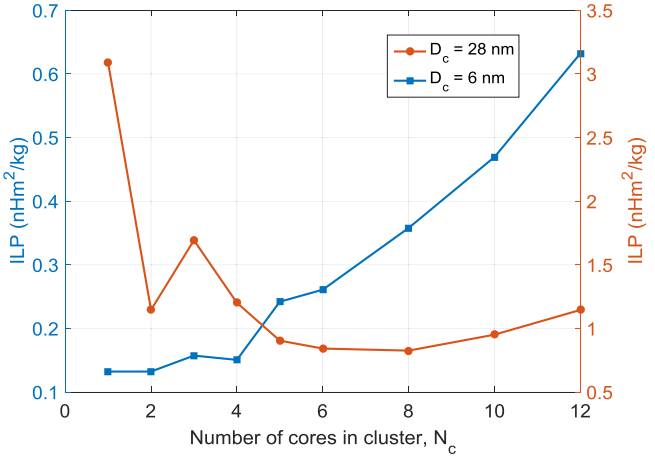

Fig. 6. Simulated ILP versus number of cores in core-cluster for two core sizes, below and above the core size that gives the maximum ILP value. Red curve $D_c = 28\,\mathrm{nm}$, blue curve $D_c = 6\,\mathrm{nm}$, $K = 10\,\mathrm{kJ/m^3}$, $M_S = 400\,\mathrm{kA/m}$, $T = 300\,\mathrm{K}$, Applied field amplitude and frequency is $B_0 = 10\,\mathrm{mT}$ and $f = 1\,\mathrm{MHz}$. Only dipole-dipole interactions included. (For interpretation of the references to colour in this figure legend, the reader is referred to the web version of this article.)

In Fig. 6 we can see an interesting behaviour. For core sizes above the size that gives the maximum in ILP, the ILP value decreases with increasing number of cores, N_c. This is expected and has also been determined from experiment [5]. However, for core sizes below the size that gives the ILP maximum the ILP value increases with increasing N_c. Both observations may be explained by the change in dipole-dipole interactions between the cores as the number of cores in the clusters change, thereby changing the Néel relaxation time with respect to the excitation frequency.

Bringing this all together, Fig. 7 shows the experimental ILP data superimposed with the calculated ILP values obtained using the non-interacting model and the MC simulations at 1 MHz, as a function of core size. It is clear that there is very good agreement across the full range of core sizes, using both models.

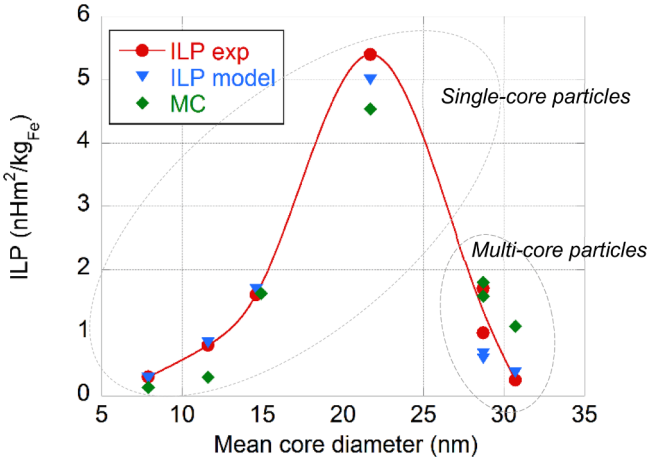

Fig. 7. Experimental ILP data determined from SAR/ILP analysis (field amplitudes between 3.4 and 9.9 kA/m and at frequency 1 MHz) (red), calculated ILP values using the non-interacting ILP model (blue) and simulated ILP using the dynamic Monte-Carlo model at 1 MHz with dipole-dipole interactions for the multi-core MNPs (green). MNP parameters used in the analysis are determined from TEM, and magnetization vs field (e.g. core size, core size distribution and saturation magnetization) and magnetic anisotropies from [21]. (For interpretation of the references to colour in this figure legend, the reader is referred to the web version of this article.)

4. Conclusions

We have investigated experimental ILP values for different iron-oxide core sizes both for single- and multi-core particles.

We have found that a non-interacting ILP model can be used when the field is not too high (as compared to $2K/M_s$). In order to include interactions (dipole-dipole and exchange interactions) and non-linear field effects, a dynamic Monte-Carlo model should be used.

Both models can explain how the ILP varies with core size and the core-core interactions in the multi-core particles, for instance the peak in ILP at a specific core size (about 20 nm) for 1 MHz.

From the analysis we have found that the core-core interactions give a different behaviour in ILP dependent on if the core size is above or below the core size that gives the maximum in ILP. This is something we will investigate further in an upcoming paper [15].

Acknowledgement

The work in this study was financed by the EU FP7 NMP project NanoMag, grant agreement no: 604448.

References

[1] Q.A. Pankhurst, J. Connolly, S.K. Jones, J. Dobson, Applications of magnetic nanoparticles in biomedicine, J. Phys. D Appl. Phys. 36 (2003) 167–181.
[2] K.M. Krishnan, Biomedical nanomagnetics: a *spin* through possibilities in imaging, diagnostics, and therapy, IEEE Trans. Magn. 46 (2010) 2523–2558.
[3] S. Dutz, R. Hergt, Magnetic particle hyperthermia — a promising tumour therapy, Nanotechnology 25 (2014) 28.
[4] J. Wells, O. Kazakova, O. Posth, U. Steinhoff, S. Petronis, L.K. Bogart, P. Southern, Q. Pankhurst, C. Johansson, Standardisation of magnetic nanoparticles in liquid suspension, J. Phys. D 50 (2017) 383003.
[5] C. Blanco-Andujar, D. Ortega, P. Southern, Q.A. Pankhurst, N.T.K. Thanh, High performance multi-core iron oxide nanoparticles for magnetic hyperthermia: microwave synthesis, and the role of core-to-core interactions, Nanoscale 7 (2015) 1768.
[6] V. Schaller, G. Wahnström, A. Sanz-Velasco, S. Gustafsson, E. Olsson, P. Enoksson, C. Johansson, Monte Carlo simulation of magnetic multi-core nanoparticles, J. Magn. Magn. Mater. 321 (2009) 1400–1403.
[7] V. Schaller, G. Wahnström, A. Sanz-Velasco, P. Enoksson, C. Johansson, Effective magnetic moment of magnetic multi-core nanoparticles, Phys. Rev. B 80 (2009) 092406.
[8] E. Wetterskog, C. Jonasson, D.-M. Smilgies, V. Schaller, C. Johansson, P. Svedlindh, Colossal anisotropy of the dynamic magnetic susceptibility in low-dimensional nanocube assemblies, ACS Nano (2018) 1403–1412.
[9] R.P. Tan, J. Carrey, M. Respaud, Magnetic hyperthermia properties of nanoparticles inside lysosomes using kinetic Monte Carlo simulations: influence of key parameters and dipolar interactions, and evidence for strong spatial variation of heating power, Phys. Rev. B 90 (2014) 214421.
[10] H.F. Du, A. Du, Effect of exchange and dipolar interactions on the hysteresis of magnetic nanoparticle systems, Phys. Stat. Sol. 244 (4) ((b) 2007,) 1401–1408.
[11] J.-O. Andersson, D. Djurberg, T. Jonsson, P. Svedlindh, P. Nordblad, Monte Carlo studies of the dynamics of an interacting monodispersive magnetic-particle system, Phys. Rev. B 56 (1997) 13983.
[12] L.C. Branquinho, M.S. Carrião, A.S. Costa, N. Zufelato, M.H. Sousa, R. Miotto, R. Ivkov, A.F. Bakuzis, Effect of magnetic dipolar interactions on nanoparticle heating efficiency: implications for cancer hyperthermia, Sci. Rep. 3 (2013) 2887.
[13] G. Salas, C. Casado, F.J. Teran, R. Miranda, C.J. Serna, M. Puerto Morales, Controlled synthesis of uniform magnetite nanocrystals with high-quality properties for biomedical applications, J. Mater. Chem. 22 (2012) 21065.
[14] M. Marciello, V. Connord, S. Veintemillas-Verdaguer, M.A. Vergés, J. Carrey, M. Respaud, C.J. Serna, M. Puerto Morales, Large scale production of biocompatible magnetite nanocrystals with high saturation magnetization values through green aqueous synthesis, J. Mater. Chem. B 1 (2013) 5995–6004.
[15] L.K. Bogart et al., On structure driven functional properties of single- and multi-core particles, in preparation.
[16] R.R. Wildeboer, P. Southern, Q.A. Pankhurst, On the reliable measurement of specific absorption rates and intrinsic loss parameters in magnetic hyperthermia materials, J. Phys. D 47 (2014) 495003.
[17] R.E. Rosensweig, Heating magnetic fluid with alternating magnetic field, J. Magn. Magn. Mater. 252 (2002) 370–374.
[18] H. Mamiya, B. Jeyadevan, Hyperthermic effects of dissipative structures of magnetic nanoparticles in large alternating magnetic fields, Sci. Rep. 1 (2011) 157.
[19] J. Dieckhoff, D. Eberbeck, M. Schilling, F. Ludwig, Magnetic-field dependence of Brownian and Néel relaxation times, J. Appl. Phys. 119 (2016) 043903.
[20] M. Osaci, M. Cacciola, An adapted Coffey model for studying susceptibility losses in interacting magnetic nanoparticles, Beilstein J. Nanotechnol. 6 (2015) 2173–2182.
[21] A. Demortiere, P. Panissod, B. Pichon, G. Pourroy, D. Guillon, B. Donnio, S. Begin-Colin, Size-dependent properties of magnetic iron oxide nanocrystals, Nanoscale 3 (2010) 225–232.
[22] M. Kallumadil, M. Tada, T. Nakagawa, M. Abe, P. Southern, Q.A. Pankhurst, Suitability of commercial colloids for magnetic hyperthermia, J. Magn. Magn. Mater. 321 (2009) 1509–1513.